Energetics of Peptide Recognition by the Second PDZ Domain of Human Protein Tyrosine Phosphatase 1E[†]

Stoyan Milev,[‡] Saša Bjelić,[‡] Oleg Georgiev,[§] and Ilian Jelesarov*,[‡]

Biochemisches Institut der Universität Zürich and Institut für Molekularbiologie der Universität Zürich, Winterthurerstrasse 190, CH-8057 Zürich, Switzerland

Received September 8, 2006; Revised Manuscript Received October 31, 2006

ABSTRACT: Formation of protein−protein assemblies is essential in maintaining cell structure and function. Conservation of structural motifs and binding sites is the result of evolutionary pressure for solutions compatible with both molecular economy and regulation. PDZ domains are a typical example: A conserved fold governs specificity toward recognition of C-terminal protein sequences by small sequential and/or structural deviations within a canonical binding mode. The energetic principles underlying the strength and specificity of PDZ−protein interactions are practically unknown. We use the second PDZ domain (PDZ2) of the human protein tyrosine phosphatase (hPTP1E) as a model to study the energetics of peptide binding to a class I PDZ domain. Calorimetric experiments reveal the enthalpy, entropy, and heat capacity changes accompanying PDZ2 binding to the C-terminal pentadecapeptide derived from the guanine nucleotide exchange factor RA-GEF2. Association is driven by favorable enthalpy and entropy changes below 18 °C. Above that temperature the entropy change opposes complex formation. Structure-based predictions poorly reproduce the observed thermodynamic profile of the PDZ−peptide complex. On the basis of MD simulations and experimental findings by others we suggest that changes in the dynamics of the PDZ domain upon peptide binding make a large contribution to the observed thermodynamic parameters. Possible impacts of subtle, ligand-induced structural "stiffening" of PDZ domains are discussed. In our hands, the C-terminal segment of the tumor suppressor APC binds much less tightly to PDZ2 than what has been proposed earlier from surface plasmon resonance experiments.

PDZ[1] domains are a family of small, evolutionary well-represented protein binding modules. Usually they are arranged in tandems and facilitate formation of multiprotein networks involved in signaling, cytoskeletal organization, and subcellular transport (*1*). Next to being "passive" scaffolds, PDZ domains can also modulate the function of partner proteins such as ion channels and membrane receptors (refs *2* and *3* and references cited therein). Mutations in genes encoding PDZ-containing proteins are linked to human diseases (*4*−*7*).

Despite low overall sequential homology the known high-resolution structures of PDZ domains exhibit only little structural variation (C_α RMSD on the order of 1.5 Å). Six β-strands form a β-sandwich with nonparallel planes. Two short α-helices pack on the edges of the β-sandwich to complement the hydrophobic core. PDZ domains recognize internal sequences of partner proteins in some cases, yet the typical binding mode is recognition of C-terminal segments. Binding takes place in a groove between strand β2 and helix α2. The peptide is fixed in an extended conformation, essentially complementing the β-sheet structure. The known PDZ/peptide structures show a conserved, canonical binding motif. The main anchoring point is the very C-terminal residue, which is invariantly hydrophobic. The apolar side chain fills the hydrophobic pocket formed between strands β2 and β3 and α-helix α2. The terminal carboxylate is coordinated by amide hydrogen bonds within a unique glycine-rich loop. Four upstream residues of the peptide ligand are typically involved in interactions with the protein. (Conventionally, sequence position 0 is assigned to the C-terminal residue of the peptide ligand and the sequence numbering is negative toward the N-terminus.) Depending on the specificity of interactions made by the residue located in position −2 of the incoming peptide with the side chain in position 1 of α-helix α2 of PDZ, three classes of PDZ domains have been defined so far (*3*). In class I PDZ, a hydrogen bond is formed between the hydroxyl group of Ser/Thr −2 and His 71. An apolar contact in this critical site defines class II PDZ. Aspartic acid or glutamic acid occupies position −2 in class III PDZ ligands. The preference is guided by the possibility of a hydrogen bond being formed between the side chain carboxylate and the hydroxyl group of tyrosine from helix α2. Examples violating this paradigm

[†] This work was supported in part by the Swiss National Science Foundation (Grant 31-100197/1).

* To whom correspondence should be addressed: phone, ++41 44 635 5547; fax, ++41 44 635 6805; e-mail, iljel@bioc.unizh.ch.

[‡] Biochemisches Institut der Universität Zürich.

[§] Institut für Molekularbiologie der Universität Zürich.

[1] Abbreviations: APC, tumor supressor adenomatous polyposis coli protein; ASA, solvent-accessible surface (in Å); ΔC_p, heat capacity change; DSC, differential scanning calorimetry; ΔG, free energy change; ΔH, enthalpy change; ITC, isothermal titration calorimetry; K_d, equilibrium dissociation constant; PDZ, postsynaptic density protein-95; PDZ2, the second PDZ domain of the human protein tyrosine phosphatase 1E (hPTP1E); RA-GEF2, guanine nucleotide exchange factor 2; ΔS, entropy change; RG, synthetic pentadecapeptide comprising the C-terminus of RA-GEF2.

10.1021/bi061869i CCC: $37.00
Published on Web 01/06/2007

are documented, and some PDZ domains exhibit degenerate specificity (*8*). Positions −1 and −3 are more solvent exposed, exhibit no preference for specific side chains, and are thought to fine-tune the specificity and possibly the affinity of interactions. In some cases the PDZ domain provides anchoring sites for residues located as far as position −7 in the peptide ligand (*9*−*13*).

Although the structural determinants governing binding of C-terminal peptides to PDZ domains are now well established, much less is known about the energetics of association. Solid-phase methods such as surface plasmon resonance and ELISA yield dissociation constants typically in the range 1−200 nM (*14*−*16*). Differently, solution methods (ITC, fluorescence, NMR) suggest that the typical binding affinity may be lower, in the micromolar range (*17*−*20*), although a K_d of 270 nM was measured recently by ITC for a RIM1α PDZ domain with unusual specificity (*21*).

We select the second PDZ domain (PDZ2) of the human tyrosine phosphatase (hPTP1E) as a model to study the energetics of peptide binding to a class I PDZ domain. hPTP1E (alternatively known as PTPbas and PTPL1) is involved in maintaining the balance of tyrosine phosphorylation and is thus implicated in the regulation of diverse receptor-mediated signal transduction pathways, among them the regulation of cell growth and apoptosis in breast cancer (*22*, *23*). The protein contains five PDZ domains. The second domain, PDZ2, is known to interact with the human Fas/CD95 receptor (*24*), the zyxin-related protein ZRP-1 (*25*), the tumor supressor adenomatous polyposis coli protein (APC), and the guanine nucleotide exchange factor RA-GEF2 (*26*). C-Terminal peptides derived from the latter two proteins were reported to bind to PDZ with $K_d = 8$ nM [APC (*14*)] and $K_d = 10-30$ μM [RA-GEF2 (*10*, *18*)], respectively.

The energetics of binding of C-terminal sequences derived from RA-GEF2 and APC proteins was characterized by isothermal titration calorimetry (ITC) and differential scanning calorimetry (DSC). The measurements confirm the low micromolar dissociation constant of the RA-GEF2-derived peptide (henceforth abbreviated as RG). Surprisingly, we found that the affinity of PDZ2 for the APC peptide is much lower than what has been suggested previously. To our knowledge, we report here for the first time the complete energetic profile of a PDZ−peptide complex. Analysis of the experimental thermodynamic parameters with respect to the predictions of semiempirical methods identifies energetic contributions from subtle structural changes in the PDZ domain induced by peptide binding.

EXPERIMENTAL PROCEDURES

Protein Cloning, Expression, and Purification. PDZ2 was PCR amplified from a human brain cDNA library by use of oligonucleotide primers designed from the DNA sequence (Genbank no. XM_172831). The primers PDZup (5′-GAATTcatatgCCTAAGCCTGGAGATATCTTTGAG-3′) and PDZdo-1 (5′-GCCggatccTCATGTTGGAGATTGTCCCTTTTCTAATAACAG-3′) contain *Nde*I and *Bam*HI sites, respectively. A stop codon was engineered into the PDZdo primer preceding the *Bam*HI site, so that a 96 amino acid fragment containing PDZ2 would be expressed. The PCR product was cloned between the *Nde*I and *Bam*HI sites of the pET21b bacterial expression vector and verified by sequencing. Overexpression of PDZ2 was achieved by growing *Escherichia coli* strain BL21(DE3) transformed with the expression vector in LB medium in the presence of ampicillin at 37 °C. Expression was induced with 1 mM isopropyl β-D-thiogalactopyranoside (IPTG) ,and the cultures were grown for an additional 4 h. Cells were harvested by centrifugation, resuspended in 50 mM sodium acetate and 10 mM EDTA, pH 5.0, and stored at −80 °C. The resuspended cells were lyzed by sonification. The supernatant was loaded on a HiTrap SP HP cation-exchange column in buffer A (50 mM sodium acetate, 10 mM EDTA, pH 5.0), and the PDZ2 domain was eluted with buffer B (50 mM sodium acetate, 10 mM EDTA, 1 M NaCl, pH 5.0). The protein was further purified by reversed-phase HPLC in binary acetonitrile/water gradients containing 0.1% and 0.085% trifluoroacetic acid on a C8 column and lyophilized. The protein which was refolded from the lyophilized state was fully native as judged by spectroscopy and scanning calorimetry. The binding parameters obtained with material after cation exchange or HPLC as the final purification step were identical. The mass was verified by ESI mass spectrometry. Concentration was calculated using $\epsilon_{280} = 2125\ M^{-1}\ cm^{-1}$ determined by quantitative amino acid analysis.

Peptide Synthesis and Purification. Peptide Ac-NH-YADSEADENEQVSAV-OH (RG) corresponding to the 15 C-terminal amino acids of guanine nucleotide exchange factor RA-GEF-2 and peptide Ac-NH-SSGTQSPKRHSG-SYLVTSV-OH (APC) corresponding to the 19 C-terminal amino acids of tumor suppressor APC were custom synthesized using the N^{α}-Fmoc protection strategy. The naturally occurring phenylalanine in RG (N-terminal residue in the pentadecapeptide) was replaced by tyrosine to facilitate concentration determination by UV. The N-terminal residue was acetylated by reaction of the resin-bound and side chain protected peptide with a 10-fold molar excess of acetic anhydride and a 5-fold molar excess of trimethylamine in dimethylformamide. After deprotection and cleavage from the resin, crude peptide preparations were desalted on a Sephadex G-25 column in 1 M acetic acid. Final purification was achieved by reversed-phase HPLC on a semipreparative C8 column eluted with binary acetonitrile/water gradients containing 0.1% trifluoroacetic acid. The purity of peptides was controlled by ESI mass spectrometry. The concentration was determined by UV absorption using $\epsilon_{280} = 1280\ M^{-1}\ cm^{-1}$.

Buffer. All experiments were conducted in standard buffer composed of 50 mM sodium phosphate and 150 mM NaCl, pH 6.8. The pH of samples containing urea was adjusted after addition of the denaturant. Urea concentrations were determined by measuring the refraction index. All chemicals were of analytical grade and were used without further purification.

Differential Scanning Calorimetry (DSC). DSC experiments were performed on a VP-DSC calorimeter (MicroCal Inc.) equipped with twin coin-shaped cells of 0.52 mL volume. Details on the instrument's performance are given elsewhere (*27*). The heating rate was 1 °C min^{-1}. Samples containing protein and peptide (in isolation or as a mixture) were dialyzed for 18−24 h against the same batch of buffer used to establish the instrumental buffer−buffer baseline. Reversibility was checked by two to three cycles of heating and cooling. The raw experimental data were corrected for

the instrumental baseline and transformed to partial molar or partial specific heat capacity using partial specific volumes of 0.724, 0.684, and 0.718 $cm^3\ g^{-1}$ for PDZ2, RG, and the PDZ2/RG mixture, respectively, calculated from the amino acid composition. The analysis of heat capacity traces of the protein−peptide complex followed the formalism detailed elsewhere (*28*−*30*). Briefly, considering the unfolding of a monomeric protein, the temperature dependence of the measured heat capacity is expressed as

$$C_p(T) = C_{p,\mathrm{N}} + f_\mathrm{U}\Delta C_p + \Delta H_\mathrm{m}\frac{\mathrm{d}f_\mathrm{U}}{\mathrm{d}T} = C_{p,\mathrm{N}} + f_\mathrm{U}\Delta C_p + \frac{K_\mathrm{U}}{(1+K_\mathrm{U})^2}\left(\frac{\Delta H_\mathrm{m}^{\,2}}{RT^2}\right) \quad (1)$$

where K_U is the equilibrium unfolding constant, $f_\mathrm{U} = K_\mathrm{U}/(1 + K_\mathrm{U})$ is the fraction of unfolded protein, ΔH_m is the unfolding enthalpy at T_m, the temperature where $f_\mathrm{U} = 0.5$ (i.e., $K_\mathrm{U} = 1$), and $\Delta C_p = C_{p,\mathrm{U}} - C_{p,\mathrm{N}}$ is the unfolding heat capacity change. The heat capacity of the folded protein, $C_{p,\mathrm{N}}$, was modeled with a linear function. As shown before, the heat capacity of the unfolded state, $C_{p,\mathrm{U}}$, can be calculated with good precision from the amino acid composition of the protein and is well approximated by a second-order polynomial function of the general form $C_{p,\mathrm{U}} = a + bT + cT^2$, where *a*, *b*, and *c* are coefficients (*31*). In eq 1, it is implicitly assumed that K_U depends on the temperature according to eq 6 below. Regression analysis according to eq 1 returns an optimized value for ΔH_m, which is in fact the geometric mean of the model-independent calorimetric enthalpy, ΔH_cal, and the model-dependent van't Hoff enthalpy, ΔH_vH, i.e., $\Delta H_\mathrm{m} = (\Delta H_\mathrm{cal}\Delta H_\mathrm{vH})^{1/2}$. For a two-state transition, $\Delta H_\mathrm{cal} = \Delta H_\mathrm{vH}$. The calorimetric enthalpy is obtained by integration of the $C_p(T)$ function above the intrinsic heat capacity change function, which is defined by the first two terms on the right-hand side of eq 1. The van't Hoff enthalpy can be calculated as $\Delta H_\mathrm{vH} = 2T_\mathrm{m}[R(C_{p,\max} - \Delta C_p/2)]^{1/2}$, where $C_{p,\max}$ is the heat capacity at T_m. Data handling and analysis were carried out using the program CpCalc 2.1 (Applied Thermodynamics), subroutines for Origin provided by MicroCal, and in-house written scripts for NLREG (Phillip H. Sherrod).

Isothermal Titration Calorimetry (ITC). ITC experiments were performed on a VP-ITC instrument (MicroCal Inc.). The calorimeter was calibrated according to the manufacturer's instruction. Samples of protein and peptide were prepared in, and thoroughly dialyzed against, the same batch of buffer to minimize artifacts due to minor differences in buffer composition. The concentration was determined after dialysis. The sample cell (1.4 mL) was loaded with 30−80 μM protein; peptide concentration in the syringe was 400−1000 μM. A titration experiment typically consisted of 25−30 injections, each of 8 or 10 μL volume and 10 or 12 s duration, with a 5 min interval between additions. The stirring rate was 300 rpm. Raw data were integrated, corrected for nonspecific heats, normalized for concentration, and analyzed according to a 1:1 binding model assuming a single set of identical binding sites.

Circular Dichroism Spectroscopy (*CD*). CD measurements were carried out on a Jasco J-715 instrument equipped with a computer-controlled water bath using jacketed cuvettes of 0.1 and 1.0 cm optical path. Isothermal urea unfolding experiments were performed at 5, 15, 25, and 35 °C. The data were analyzed following the linear extrapolation model (LEM) as detailed elsewhere (*32*). The ΔG_U values measured at different temperatures define the stability curve of the protein according to the Gibbs−Helmholtz equation:

$$\Delta G_\mathrm{U}(T) = \Delta H_\mathrm{R}\left(1 - \frac{T}{T_\mathrm{R}}\right) + \Delta C_p\left[T - T_\mathrm{R} - T\ln\left(\frac{T}{T_\mathrm{R}}\right)\right] \quad (2)$$

Conveniently, T_R is selected as the temperature where the protein is half unfolded ($f_\mathrm{U} = 0.5$ and $\Delta H_\mathrm{U} = \Delta H_\mathrm{R}$). For monomeric proteins, if T_R is known from an independent experiment (thermal unfolding), $\Delta G(T_\mathrm{R}) = -RT\ln[f_\mathrm{U}/(1 - f_\mathrm{U})] = 0$ can be included in the data set to reduce the uncertainty when three parameters are being optimized based on (usually) few experimental points collected at low temperatures.

Binding Simulations. To simulate the temperature dependence of the excess heat capacity function of a mixture of protein and peptide, the theoretical framework developed by Brandts and Lin was used (*33*). We assume that a 1:1 complex between protein and peptide is formed; the peptide binds only to folded protein. The relevant equilibria to be considered are

$$\mathrm{PDZ_F} + \mathrm{RG} \overset{K_\mathrm{A}}{\rightleftharpoons} \mathrm{PDZ_F/RG}$$

$$\mathrm{PDZ_F} \overset{K_\mathrm{U}}{\rightleftharpoons} \mathrm{PDZ_U}$$

The equilibrium association constant, K_A, and the equilibrium unfolding constant are defined in the usual way as

$$K_\mathrm{A} = \frac{[\mathrm{PDZ_F/RG}]}{[\mathrm{PDZ_F}][\mathrm{RG}]} \quad (3)$$

$$K_\mathrm{U} = \frac{[\mathrm{PDZ_U}]}{[\mathrm{PDZ_F}]} \quad (4)$$

The brackets indicate the equilibrium concentrations of folded unbound protein ($\mathrm{PDZ_F}$), unfolded protein ($\mathrm{PDZ_U}$), unbound peptide (RG), and the complex ($\mathrm{PDZ_F/RG}$). The temperature dependencies of K_A and K_U are given by

$$K_\mathrm{A}(T) = K_{\mathrm{A,R}}\exp\left[-\frac{\Delta H_{\mathrm{A,R}}}{R}\left(\frac{1}{T} - \frac{1}{T_\mathrm{R}}\right) + \frac{\Delta C_{p,\mathrm{A}}}{R}\left(\ln\frac{T}{T_\mathrm{R}} + \frac{T_\mathrm{R}}{T} - 1\right)\right] \quad (5)$$

$$K_\mathrm{U}(T) = \exp\left[-\frac{\Delta H_\mathrm{m}}{RT}\left(1 - \frac{T}{T_\mathrm{m}}\right) - \frac{\Delta C_p}{RT}\left(T - T_\mathrm{m} - T\ln\frac{T}{T_\mathrm{m}}\right)\right] \quad (6)$$

$K_{\mathrm{A,R}}$ and $\Delta H_{\mathrm{A,R}}$ are the binding constant and the binding enthalpy change at the reference temperature T_R, which was taken as 298.15 K (25 °C), and $\Delta C_{p,\mathrm{A}} = \mathrm{d}\Delta H_\mathrm{A}/\mathrm{d}T$ is the heat capacity change of association. Parameters which characterize unfolding of the protein [ΔH_m, ΔC_p, and T_m = 322.6 K (49.4 °C)] are defined as in eq 2. At any temperature,

the enthalpy and heat capacity changes can be calculated from

$$\Delta H_A = \Delta H_{A,R} + \Delta C_{p,A}(T - T_R) \quad (7)$$

$$\Delta H_U = \Delta H_m + \Delta C_p(T - T_m) \quad (8)$$

The mass conservation equations link the two equilibria. For the total protein (PDZ_T) and peptide (RG_T) concentration we can write

$$[PDZ_T] = [PDZ_F] + [PDZ_U] + [PDZ_F/RG] = [PDZ_F] + K_U[PDZ_F] + K_A[PDZ_F][RG] \quad (9)$$

$$[RG_T] = [RG] + [PDZ_F/GR] = [RG] + K_A[PDZ_F][RG] \quad (10)$$

Since PDZ_T and RG_T are known, the combined eqs 3−10 can be solved simultaneously to determine the concentrations of the relevant species at any temperature:

$$[PDZ_F] = [PDZ_T]/(1 + K_U + K_A[RG]) \quad (11)$$

$$[PDZ_U] = K_U[PDZ_T]/(1 + K_U + K_A[RG]) \quad (12)$$

$$[PDZ_F/RG] = K_U[RG][PDZ_T]/(1 + K_U + K_A[RG]) \quad (13)$$

Taking the protein−peptide complex as the reference state, the excess enthalpy function, $\langle \Delta H \rangle$, is defined as

$$\langle \Delta H \rangle = \Delta H_U \frac{[PDZ_U]}{[PDZ_T]} - \Delta H_A \frac{[PDZ_F] + [PDZ_U]}{[PDZ_T]} \quad (14)$$

The minus sign accounts for complex dissociation. Numerical differentiation of eq 14 yields the temperature dependence of the excess heat capacity function.

Electrostatic Modeling. The free protein was modeled either with the structure extracted from the NMR ensemble of the complex or with the NMR ensembles of the free human PDZ2 (3PDZ) and the free mouse homologue (1GM1; 94% sequence identity). Ten conformers of the corresponding NMR ensembles were used. The calculation was done with the Poisson−Boltzmann model in the framework of the continuum approximation, as implemented in the program MEAD (*34*).

Molecular Dynamics Simulations. The MD simulations were carried out with the GROMACS simulation suite (version 3.3.1) (*35*) using the OPLS all-atom force field. Models 1 and 20 of the NMR ensemble (1D5G) were used as the starting point for MD simulation. The clashes in the structure were removed with the WHATIF program (http://swift.cmbi.kun.nl/WIWWWI/). The structure (complex, protein, or peptide) was solvated with TIP4 water (*36*), including approximately 150 mM NaCl (plus additional ions to neutralize the total system). A cubic periodic box was chosen such that the minimum distance between the protein and the end of the box was more the 15 Å. After minimization using the steepest descent algorithm with a tolerance of 100 kJ mol^{-1} $Å^{-1}$, the system solvent was relaxed for 500 ps with a harmonic position restraint on all C_α atoms (force constant: 10 kJ mol^{-1} $Å^{-2}$). LINCS (*37*) and SETTLE (*38*) algorithms were applied for constraining the bond lengths. The integration step was 2 fs. Short-range electrostatics were calculated explicitly, and long-range electrostatic interactions were calculated using the particle-mesh Ewald method (*39*). A 10 Å cutoff was used for van der Waals interactions. A long-range correction for the energy and the pressure was applied. The system was coupled to a Berendsen temperature bath ($\tau_t = 0.1$ ps), separately for the protein and the solvent, and to a Berendsen pressure bath ($\tau_p = 0.1$ ps) (*40*). The simulations were performed at 300 K. The simulation time was 15 ns. Trajectory visualization and analyzing was made with the visualization and analyzing software VMD.

Structural Parametrization. In the following we briefly describe the methods used for calculating of energetic terms based on the structure of the PDZ2/RG complex. Detailed discussion can be found elsewhere (*41*, *42*). Solvent-accessible surface (ASA) calculations were performed with the program NACCESS using a probe radius of 1.4 Å and a slice width of 0.25 Å, the default set of atomic radii (*43*). From each trajectory, the average ASA was calculated as the arithmetic mean over ASAs of equally distant snapshots (step 20 ps) taken in the last 10 ns of simulation. The ensemble-averaged differences in ASA between the associated and dissociated state (ΔASA) was partitioned into polar (ΔASA_{pol}) and apolar (ΔASA_{apol}) components. The hydration contribution to the binding heat capacity (ΔC_p) is calculated by

$$\Delta C_p = \sum C_{p,i} \Delta ASA_i \quad (15)$$

where the terms ΔASA are in units of $Å^2$ and the coefficients $C_{p,i}$ are the elementary contributions (in units of kJ K^{-1} mol^{-1} $Å^{-2}$) to the heat capacity of hydration of the corresponding type of surface. The following $C_{p,i}$ values were used: $C_{p,apol} = 1.82$, $C_{p,pol} = -1.09$, and $C_{p,OH} = 0.71$ (the last term accounts for the heat capacity contribution of buried hydroxyl groups of serine and threonine). In the absence of proton release/uptake upon complex formation, the generic binding enthalpy at 60 °C can be calculated within an estimated error range of 10% as (in kJ mol^{-1}):

$$\Delta H^{60°}_{calc} = 122\Delta ASA_{pol,i} - 30.4\Delta ASA_{apol} \quad (16)$$

At any other temperature the binding enthalpy is determined using $\Delta H^{60°}$ and the calculated ΔC_p.

It has naturalized itself to partition the binding entropy change into three terms describing (i) the entropy of water reorganization caused by the change in molecular surface (ΔS_{hyd}), (ii) the loss of conformational entropy due to side chain and backbone immobilization (ΔS_{conf}), and (iii) the change of rotational/translational degrees of freedom when two free kinetic units form the bimolecular complex (ΔS_{rt}):

$$\Delta S = \Delta S_{hyd} + \Delta S_{conf} + \Delta S_{rt} \quad (17)$$

The change in hydration entropy is calculated by extrapolation, using ΔC_p and the temperatures where the hydration entropy of polar and apolar atoms is zero (335.15 and 385.15 K, respectively):

$$\Delta S_{hyd} = C_{p,apol}\Delta ASA_{apol} \ln\left(\frac{T}{385.15}\right) + C_{p,pol}\Delta ASA_{pol} \ln\left(\frac{T}{335.15}\right) \quad (18)$$

The calculation of the ΔS_{conf} term of eq 17 poses a major problem in estimating energetics from structural data. According to the method used here, the side chain entropy loss can be estimated from the change in ASA_i upon binding:

$$\Delta S_{conf,SC} = \sum_i \frac{\Delta ASA_i}{ASA_{AXA,i}} \Delta S_{bu-ex,i} \qquad (19)$$

$ASA_{AXA,i}$ is ASA of the corresponding side chain in the fully exposed state (modeled as Ala-X-Ala), and $\Delta S_{bu-ex,i}$ is the entropy loss for a complete burial of the side chain of type i. Residues immobilized in the binding pocket experience loss of conformational entropy from backbone immobilization (ΔS_{bb}). An additional term (ΔS_{ex-u}) represents the unfavorable change in entropy for side chains which are solvent exposed but structured in the protein−peptide complex. The values of $ASA_{AXA,i}$, $\Delta S_{bu-ex,i}$, ΔS_{bb}, and ΔS_{ex-u} were taken from ref *41*.

The magnitude of ΔS_{rt} is still uncertain (ref *44* and cited work therein). We use here $\Delta S_{rt} = -35$ J K^{-1} mol^{-1}. This number is numerically close to the "cratic entropy" and has been found to describe reasonably the loss of rotational/translational degrees of freedom in diverse experimental systems (*44*−*46*).

RESULTS AND DISCUSSION

PDZ2 was expressed in soluble form in the cytoplasm of *E. coli*. The purified protein is monomeric at the concentrations and under the experimental conditions used in this study, as evidenced by light scattering experiments. The far-UV CD spectrum has the spectral signature of proteins containing predominantly β-sheets. CD spectroscopy demonstrates that the two peptides used in this study adopt a random coil conformation in solution (not shown). We first describe thermal and isothermal urea-induced unfolding experiments aimed at determination of the thermodynamic stability and clarification of the unfolding mechanism of PDZ2. This information is important in order to confine binding experiments in the temperature range where PDZ2 is fully native, as well as to interpret the results from thermal melting of the protein−peptide complex. ITC and DSC experiments revealing the energetics of peptide binding to the protein are presented in the second part. In the third part we search for correlations between the observed thermodynamic parameters and the structural features of the PDZ2/RG complex.

Stability and Unfolding Energetics of PDZ2. (A) Thermal Unfolding. The thermodynamic stability and unfolding mechanism of PDZ2 were characterized by DSC (Figure 1). The partial molar heat capacity at 25 °C is 15.6 ± 1.0 kJ K^{-1} mol^{-1}, corresponding to a partial specific heat capacity of 1.56 ± 1.00 J K^{-1} g^{-1}. This value is typical for globular proteins (*47*). Between 5 and 30 °C, the heat capacity increases linearly with a slope $dC_p/dT = 0.107 \pm 0.005$ kJ K^{-2} mol^{-1}, corresponding to $(10.7 \pm 0.5) \times 10^{-3}$ J K^{-2} g^{-1}. Although not extraordinarily steep in comparison with compact globular proteins (*47*), this increase indicates some degree of flexibility, possibly caused by thermal fluctuations of the disordered N- and C-termini (*10*). The heat capacity at 75 °C closely matches the predicted heat capacity based on summation of the heat capacities of the constituent amino acids (*31*). Hence, thermal unfolding results in a highly hydrated state lacking residual tertiary interactions. Integration of the heat absorption peak above the chemical baseline connecting the pretransitional and posttransitional heat capacities in proportion to the extent of unfolding yields the model-independent, calorimetric parameters characterizing PDZ2 unfolding: $T_{m,P} = 49.4$ °C, $\Delta H_{cal,P}(T_m) = 273 \pm 10$ kJ mol^{-1}, $\Delta S_{cal,P}(T_m) = 846 \pm 30$ J K^{-1} mol^{-1}, and $\Delta C_{p,P} = 4.45 \pm 0.40$ kJ K^{-1} mol^{-1} (Table 1). From a pH-induced variation of ΔH_m in a limited range of T_m, Gianni et al. estimated $\Delta C_p = 5.0 \pm 0.6$ kJ K^{-1} mol^{-1} for the PDZ2 Y43W mutant (*48*). The specific unfolding parameters at 60 °C are $\Delta H_{cal,P}(60) = 3.3 \pm 2$ kJ mol res^{-1}, $\Delta S_{cal,P}(60) = 10.3 \pm 0.5$ J K^{-1} mol res^{-1}, and $\Delta C_{p,P} = 46 \pm 2$ J K^{-1} mol res^{-1} and are well within the range of values determined for globular proteins (*49*, *50*). Altogether, the calorimetric data imply that PDZ2 is a compact globular domain.

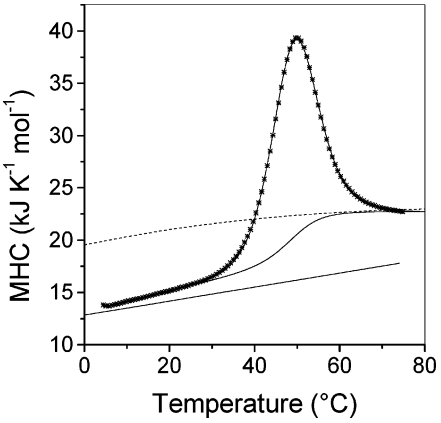

FIGURE 1: Thermal unfolding of PDZ2 observed by DSC. The experimentally measured temperature dependence of the partial molar heat capacity function is shown with symbols (average of three individual scans). The intrinsic heat capacity change (chemical baseline; continuous line below the heat absorption peak) was calculated as $C_{p,base} = (1 - f_U)C_{p,N} + f_U C_{p,U}$, where $C_{p,N}$ and $C_{p,U}$ are the heat capacities of the native state and of the unfolded state, respectively, and f_U is the fractional amount of heat absorbed between 30 and 75 °C. The heat capacity of the denatured state calculated by summation of the heat capacities of the constituent amino acids is indicated by the dotted line. The straight line represents the heat capacity of an average native globular protein with the mass of PDZ2. The line associated with the symbols visualizes the result of the nonlinear least-squares regression analysis. Statistically indistinguishable fits were obtained assuming a two-state transition ($\Delta H_{fit} = 256 \pm 10$ kJ mol^{-1}) or non-two-state transition ($\Delta H_{cal} = 273 \pm 10$ kJ mol^{-1}, $\Delta H_{vH} = 240 \pm 10$ kJ mol^{-1}). ΔH_{fit} is identical within error with the weighted enthalpy estimate, $\Delta H_{WA} = 0.65\Delta H_{vH} + 0.35\Delta H_{cal} = 251 \pm 14$ kJ mol^{-1}. Experiments were performed with 130−220 μM protein in 50 mM sodium phosphate and 150 mM NaCl, pH 6.8.

Analysis of the molar heat capacity function indicates an apparent small deviation from the two-state unfolding behavior. The temperature dependence of the excess heat capacity is best described by the model-dependent van't Hoff enthalpy $\Delta H_{vH} = 240 \pm 10$ kJ mol^{-1}. Thus the ratio $\Delta H_{vH,DSC}/\Delta H_{cal}$ is 0.89 ± 0.06. However, thermodynamic modeling failed to detect the presence of statistically robust intermediates. We assume, therefore, that the apparent deviation from the two-state model is caused by accumulation of experimental errors. On the other hand, it has been proposed that a substantial improvement in the accuracy of ΔH at T_m can be achieved using a weighted enthalpy average, which is calculated as $\Delta H_{WA} = 0.65\Delta H_{vH} + 0.35\Delta H_{cal}$ (*51*).

Table 1: Thermodynamic Parameters Determining the Stability of PDZ2[a]

T	ΔH	ΔS	ΔC_p	ΔG	$U_{1/2}$	$-m_{eq}$
5[b]				22.1 ± 1.6	3.2 ± 0.1	6.9 ± 0.5
8[c]				21.7 ± 2.1	2.1[c]	10[c]
15[b]				19.2 ± 2.6	2.94 ± 0.14	6.52 ± 0.9
25[b]				14.6 ± 1.3	2.65 ± 0.12	5.52 ± 0. 5
35[b]				10.6 ± 1.3	2.11 ± 0.17	4.99 ± 0.6
49.4[d]	273 ± 10[e]	0.846 ± 0.030[e]	4.45 ± 0.40[e]	0 ± 14[e]		
	240 ± 10[f]					
	251 ± 14[g]					
	255 ± 32[h]		4.35 ± 1.90[h]			

[a] All experiments in standard buffer, 50 mM sodium phosphate and 150 mM NaCl, pH 6.8. ΔH and ΔG in units of kJ mol^{-1}; ΔS and ΔC_p in units of kJ K^{-1} mol^{-1}; $U_{1/2}$ in units of M; m_{eq} in units of kJ mol^{-1} M^{-1}. [b] From urea-induced unfolding measured by circular dichroism. [c] From GdmCl-induced unfolding measured by fluorescence (*17*). $U_{1/2}$ and m_{eq} are rough estimates taken from the corresponding plot in this paper. [d] From DSC. [e] Calorimetric estimate. [f] van't Hoff estimate. [g] Calculated as $0.65\Delta H_{vH} + 0.35\Delta H_{cal}$. [h] Calculated as the fitting parameter in the Gibbs−Helmholtz equation.

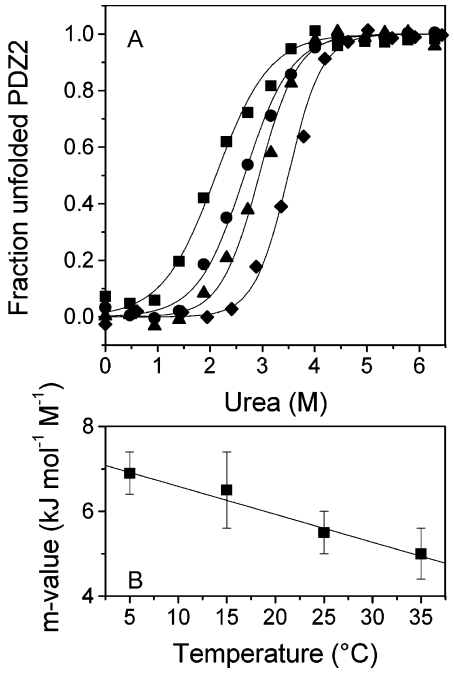

FIGURE 2: PDZ2 unfolding induced by urea-monitored CD spectroscopy. (A) Fraction of unfolded protein at 5 °C (diamonds), 15 °C (triangles), 25 °C (circles), and 35 °C (squares). The lines are the best fits from nonlinear regression analysis according to the linear extrapolation model (LEM). (B) Temperature dependence of the *m*-values obtained from LEM analysis. The regression line has a slope dm/dT = 0.066 ± 0.007 kJ mol^{-1} M^{-1} K^{-1}.

Indeed, as shown illustrated in Figure 1 ΔH_{WA} simulates perfectly the experimental trace.

(B) Urea-Induced Unfolding. The stability of PDZ2 at 5, 15, 25, and 35 °C was assessed from isothermal urea-induced unfolding experiments by following the change in ellipticity at 219 nm. The data could be modeled with a two-state transition between native and unfolded protein (Figure 2). Both the midpoints of transition, $U_{1/2}$, and the equilibrium *m*-value, $m_{eq} = -d\Delta G_{urea}/d[urea]$, depend on the temperature with slopes $dU_{1/2}/dT = -0.040 \pm 0.008$ M K^{-1} and $dm_{eq}/dT = 0.066 \pm 0.007$ kJ mol^{-1} M^{-1} K^{-1}, respectively. The mean m_{eq} (~6 kJ mol^{-1} M^{-1}) corresponds very well with the prediction of statistical analysis correlating changes of solvent-accessible surface with the magnitude of the experimental *m*-value (*52*). The unfolding free energy estimates at zero urea concentration, ΔG_U(W), calculated according to the linear extrapolation procedure are listed in Table 1.

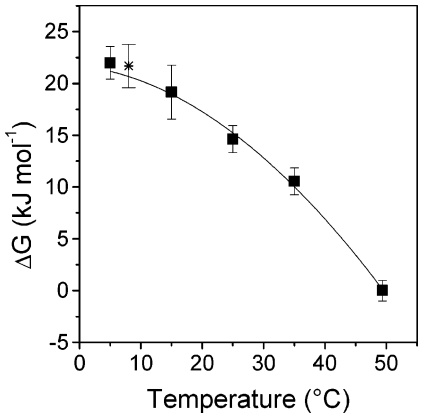

FIGURE 3: Stability curve of PDZ2. The unfolding free energies obtained by isothermal urea-induced unfolding between 5 and 35 °C were combined with $\Delta G_U = 0$ at 49.4 °C (the midpoint of thermal unfolding), and the Gibbs−Helmholtz equation was fit to the data to optimize the values for T_m, ΔH_m, and ΔC_p. The continuous line represents the best fit obtained with the following parameters: $T_m = 49.5 \pm 1.0$ °C, $\Delta H_m = 255 \pm 30$ kJ mol^{-1}, and $\Delta C_p = 4.36 \pm 1.90$ kJ K^{-1} mol^{-1}. The asterisks represent ΔG_U obtained from GdmCl-induced unfolding followed by fluorescence at 8 °C (*17*)

(C) Stability Curve of PDZ2. The Gibbs−Helmholz equation (eq 2) was fit to the combined data from thermal and urea-induced unfolding to calculate the PDZ2 stability curve (Figure 3). The best fit was obtained with the following parameters: $T_{m,fit} = 49.5 \pm 1.0$ °C, $\Delta H_{m,fit} = 255 \pm 30$ kJ mol^{-1}, and $\Delta C_{p,fit} = 4.35 \pm 1.90$ kJ K^{-1} mol^{-1} (Table 1). The correspondence between the ΔC_p and ΔH values obtained by considering data in a broad temperature range and ΔC_p and ΔH_{WA} measured directly by DSC is excellent. The only one previous estimate of PDZ2 stability is 21.7 ± 2.1 kJ mol^{-1} at 8 °C and was obtained by GdmCl-induced denaturation followed by the intrinsic changes in PDZ2 fluorescence (*17*). As shown in Figure 3, the agreement of this value with the calculated stability curve is very good. The coincidence of ΔG_U measured by three different methods is a very strong argument that PDZ2 unfolding closely obeys the two-state model. The fraction of unfolded protein is less than 1% between 5 and 30 °C. ITC experiments were performed in this temperature range.

Energetics of RG and APC Binding to PDZ2. (A) Thermodynamic Parameters Deduced from ITC. Addition of aliquots of the RG peptide to PDZ2 in the calorimetric cell produces measurable heat effects, which saturate as the

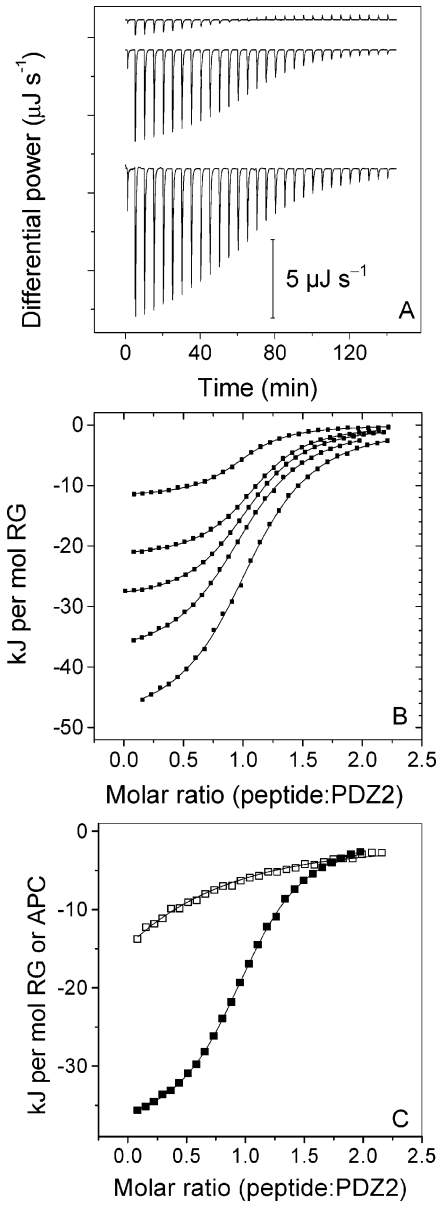

FIGURE 4: ITC binding experiments. All experiments were performed in 50 mM sodium phosphate and 150 mM NaCl, pH 6.8. The PDZ concentration in the cell was 30−80 μM; the peptide concentration in the syringe was 400−1000 μM. (A) Raw calorimetric output from experiments with the RG peptide. Experiments at 5, 18, and 30 °C are shown (top to bottom). The thermograms were shifted on the *Y*-axis for clarity. (B) Binding isotherms describing formation of the PDZ2/RG complex at 5, 12, 18, 25, and 30 °C (top to bottom). Symbols represent the integrated heats after normalization for the molar concentration. Continuous lines are nonlinear fits for a 1:1 binding model. (C) Comparison of the binding isotherms obtained at 25 °C with peptide APC (top trace and open symbols) and RG (bottom trace and filled symbols).

molar ratio of peptide to PDZ2 increases (Figure 4). From the shape of the titration curve, the binding stoichiometry, *n*, the association constant, K_A, and the apparent calorimetric enthalpy of association, ΔH_A, were calculated. The stoichiometry was 0.98 ± 0.10 (mean ± SD of 15 experiments), in agreement with a 1:1 complex seen in the NMR structure. The association constant at 25 °C is (1.94 ± 0.17) × 10^5 M^{-1}. The corresponding dissociation constant is thus ~5 μM. This first, direct, in-solution equilibrium measurement of the binding affinity of PDZ2 for RG C-terminal sequences confirms the results of two previous studies, which estimated the dissociation constant of the PDZ2/RG complex as being lower than 30 μM based on chemical shifts and amide exchange rates followed by NMR spectroscopy (*10*, *18*). From the rates of association and dissociation of the C-terminal RA-GEF2 pentapeptide to and from the PDZ2 Y43W mutant, a K_d = 6.5 ± 1.5 μM was calculated (*53*). To our knowledge, there are three published studies in which binding of C-terminal sequences to PDZ was characterized by titration calorimetry (*19*, *21*, *54*). The third PDZ domain (class I) of the PSD-95 protein binds the hexapeptide KKETEV with K_d ~ 2 μM (*54*). Dissociation constants in the range 200 nM to 50 μM characterize binding of short peptides to full-length syntenin or its PDZ tandem (*19*). An ELKS1b-derived peptide binds with high affinity (K_d = 270 nM) to the RIM1 PDZ domain (*21*).

PDZ2 was reported to bind the C-terminal stretch of the APC protein with low nanomolar affinity (*14*). We performed ITC experiments with a synthetic peptide encompassing the last 19 amino acids of the APC protein. Figure 4C compares experiments with RG and APC peptides at identical conditions. Much to our surprise, the obtained isotherms with APC are compatible with a K_d above 50 μM. The reason for this striking discrepancy with the results of Erdmann et al. is not clear at present. The vast majority of data indicating low micromolar to nanomolar affinities of PDZ domains to other proteins was collected by surface plasmon resonance experiments, and K_d's were calculated from the rates of association and dissociation (*15*, *16*, *55*). It has been demonstrated that rebinding to the sensor surface might lead to understimates of the genuine dissociation rate constant and might thus cause an overestimation of the binding affinity (*56*, *57*). In particular, next to high surface coverage, fast association rates might make rebinding very effective. Fast association is expected for ligands with relatively low steric requirements, and this is possibly the case for peptide binding to PDZ domains, since the intermolecular interface is relatively small. On the other hand, the experiments reported by Erdmann et al. were performed with a GST-PDZ2 at pH 7.4 in the presence of small amounts of nonionic detergent, and direct comparison between the two studies has to be done with caution. Nevertheless, our data demonstrate that the RA-GEF2-derived peptide binds much more strongly to isolated PDZ2 than the APC-derived peptide under identical experimental conditions. It remains to be seen in how far the differences in affinity can be related to the sequential differences at position −1 (Ala in RG versus Ser in APC) and beyond position −3, where peptide library studies indicated a preference for polar and (predominantly) negatively charged side chains (*16*). This pattern is clearly evident in RG while positions −4 and −5 are occupied by leucine and tyrosine in APC. In the context of the cell, the strength of the PDZ2/APC interaction may turn to be an important issue, since APC binding to the hPTP1E protein appears to modulate the steady-state levels of tyrosine phosphorylation of proteins playing a role in the regulation of cell division, migration, and cell adhesion (*14*).

The thermodynamic parameters characterizing the PDZ2/RG interactions are summarized in Table 2 and are presented in graphical form in Figure 5. K_A exhibits a small but statistically significant temperature variation, decreasing from (4.70 ± 0.84) × 10^5 M^{-1} at 5 °C to (1.80 ± 0.23) × 10^5 M^{-1} at 30 °C. The free energy of association is almost

Table 2: Thermodynamic Parameters Characterizing RG Binding to PDZ2 Measured by ITC[a]

T (°C)	$K_A \times 10^{-5}$ (M^{-1})	ΔG (kJ mol^{-1})	ΔH (kJ mol^{-1})	$T\Delta S$ (kJ mol^{-1})	ΔS (J K^{-1} mol^{-1})
5	4.70 ± 0.84	−30.2 ± 0.2	−11.7 ± 0.7	18.5 ± 0.2	66.5 ± 0.7
12	3.04 ± 0.23	−29.9 ± 0.1	−20.6 ± 1.4	9.3 ± 1.3	32.7 ± 0.4
18	2.63 ± 0.26	−30.2 ± 0.1	−29.1 ± 1.6	1.1 ± 1.6	3.8 ± 5.0
25	1.94 ± 1.69	−30.2 ± 0.1	−39.6 ± 0.9	−9.4 ± 0.9	−31.6 ± 3.0
25[b]	1.63 ± 0.30	−29.8 ± 0.2	−40.2 ± 3.0	−10.5 ± 3.0	−35.1 ± 17.0
25[c]	1.60 ± 0.20	−29.7 ± 0.2	−38.9 ± 2.0	−9.2 ± 2.0	−30.9 ± 6.7
30	1.80 ± 0.23	−30.5 ± 0.1	−47.3 ± 2.2	−16.8 ± 2.2	−55.4 ± 7.0
55[d]	0.18 ± 0.4	−26.8 ± 50	−80 ± 40	−53.2 ± 30.0	−162 ± 100

[a] All experiments were performed in 50 mM sodium phosphate and 150 mM NaCl, pH 6.8, unless otherwise indicated. [b] Experiment in MES buffer. [c] Experiment in Bis-Tris buffer. [d] Deduced from DSC experiments as described in the text.

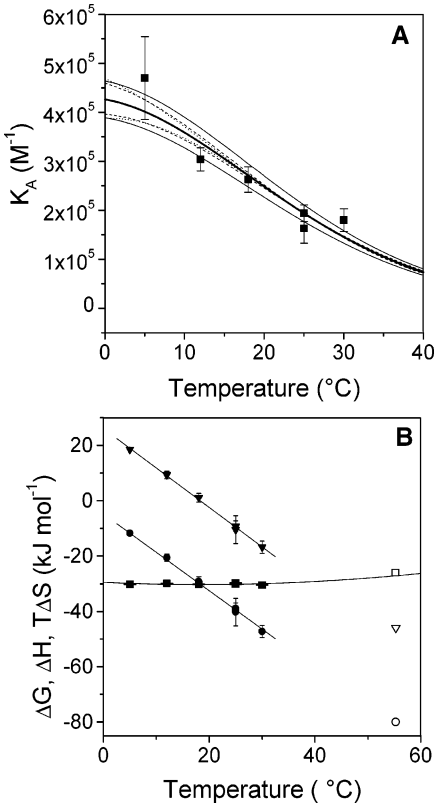

FIGURE 5: Energetics of RG binding to PDZ2 measured by ITC. All numerical values are listed in Table 2. (A) Temperature dependence of the association constant, K_A. Symbols represent the experimental data. The thick continuous line is the calculated temperature dependence of K_A, calculated according to eq 9 using as reference the data at 25 °C: $K_A = 1.94 \times 10^5$ M^{-1}, $\Delta H_A = -39.6$ kJ mol^{-1}, and $dC_{p,A} = -1.4$ kJ K^{-1} mol^{-1}. The pairs of lines illustrate the influence of the experimental uncertainty (as upper and lower limits) on the calculated temperature variation of K_A. Key: thin continuous lines, $K_A \pm 1.69 \times 10^4$ M^{-1} at fixed ΔH_A and $\Delta C_{p,A}$; dotted lines, $\Delta C_{p,A} \pm 0.2$ kJ K^{-1} mol^{-1} at fixed K_A and ΔH_A; dashed lines, $\Delta H_A \pm 2$ kJ mol^{-1} at fixed K_A and $\Delta C_{p,A}$. (B) Temperature variation of ΔG_A (squares), ΔH_A (circles), and $T\Delta S_A$ (triangles). The continuous lines associated with ΔH_A and $T\Delta S_A$ data points are linear regression lines. The line associated with the ΔG_A data points was calculated as $\Delta G_A = -RT \ln K_A$ using the simulated temperature variation of K_A (thick line in panel A). The open symbols are ΔH_A and $T\Delta S_A$ derived from DSC experiments at 55 °C.

constant in the studied range of temperatures. The apparent enthalpy changes, ΔH_A, and entropy changes, $T\Delta S_A$, of association vary with temperature. Complex formation is exothermic above 0 °C. The same ΔH_A was measured in MES and Bis-Tris buffers having different heats of protonation. It follows that there is no (net) proton release/uptake accompanying binding. The same conclusion was reached also by Saro et al. for the PSD-95 protein PDZ3 domain, another member of class I (*54*). A pK_a shift of ~1 pH unit upon binding was reported earlier for His 71, which is located at the PDZ2 binding site and forms a hydrogen bond with the hydroxyl group of Ser −2 of a Fas-derived peptide (*17*). This interaction is canonical for class I PDZ domains and, not surprisingly, is seen also in the PDZ2/RG structure. However, the measured lack of ΔH_A variation with the buffering species implies that His 71 is deprotonated both in free PDZ2 and in the PDZ2/RG complex. To further clarify the problem, we calculated the pK_a's of titratable groups in the free and peptide-bound PDZ2. The pK_a of His −71 is very low, 2.4 ± 1.2, reflecting the almost complete burial of the side chain upon peptide binding and the strong interaction with the hydroxyl group of Ser −2 of the incoming peptide. However, the pK_a of His −71 is downshifted also in the free protein. Depending on the choice of dielectric constant describing the dielectric properties of the protein, the calculated pK_a's of the unbound form vary between ~4 ($\epsilon = 4$) and ~5 ($\epsilon = 20$). The downward shift of the pK_a of the unbound form relative to the model pK_a (6.6 in this implementation) appears to be dominated by the desolvation term and interactions with permanent charges of the protein multipole and, to a lesser extent, by interactions with other titratable sites. As a control, we checked the pK_a's of the three other histidine side chains, which are not involved in interactions with RG. They are all in the range 6−7 and, most importantly, are not influenced by the presence of the peptide in the binding pocket. The calculations suggest that binding at pH 6.8 is not accompanied by proton release, in accord with the available experimental evidence.

The entropy of complex formation is positive below about 18 °C and negative at higher temperature (Figure 5). Hence, binding is favored enthalpically at all temperatures, whereas it is opposed by entropy above 18 °C. The temperature variation of the binding enthalpy, $d\Delta H_A/dT$, represents the heat capacity change of association, $\Delta C_{p,A}$. Linear regression of the data shown in Figure 5 yields $\Delta C_{p,A}$ of -1.44 ± 0.20 kJ K^{-1} mol^{-1}.

(B) DSC Studies. Further details on the binding energetics can be extracted from DSC experiments. The temperature-induced conformational transition of the preformed PDZ2/RG complex is highly reversible. The partial molar heat capacity function is shown in Figure 6 together with the traces recorded for the isolated components. The heat capacity of the RG peptide changes negligibly upon heating and is very close to the heat capacity calculated for an unstructured, completely hydrated peptide with the RG sequence. Melting of the complex produces a single heat

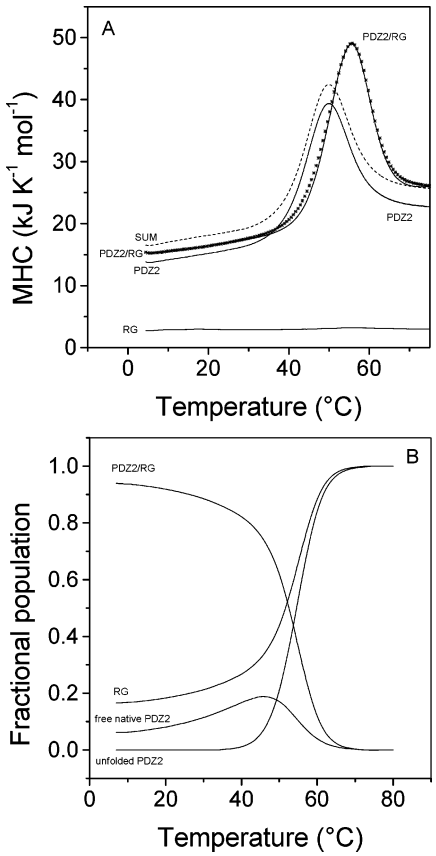

FIGURE 6: Heat capacity curves of the PDZ2/RG complex and the isolated components. (A) Thermograms recorded in standard buffer, 50 mM sodium phosphate and 150 mM NaCl, pH 6.8, at a heating rate of 1 deg min^{-1}. The labels associated with the heat capacity functions indicate experiments with the isolated RG peptide (trace RG; concentration was 250 μM), isolated protein (trace PDZ2; concentration was 222 μM), and a mixture of protein and peptide (trace PDZ2/RG shown with symbols; concentrations were 222 μM protein and 250 μM peptide). For experimental reasons, the highest concentration in DSC experiments was ~0.5 mg mL^{-1}, and precise determination of the absolute heat capacity was not possible. However, the deviation from the predicted heat capacity was only ~0.5 kJ mol^{-1} K^{-1}. The trace was therefore shifted as to match the calculated heat capacity at 75 °C. The trace labeled SUM (dashed line) is the algebraic sum of the heat capacities of the isolated components; i.e., SUM = RG + PDZ2. This is the expected heat capacity if the system was in the hypothetical dissociated state at all temperatures. The continuous line associated with experiment PDZ2/RG visualizes the result of simulation according to eqs 3−14. The curve is defined by the following parameters: K_A(25 °C) = 2.2 × 10^5 M^{-1}, ΔH_A(25 °C) = −35.5 kJ mol^{-1}, $\Delta C_{p,A}$ = −1.7 kJ K^{-1} mol^{-1}, $\Delta H_{m,P}$(49.4 °C) = 260 kJ mol^{-1}, and $\Delta C_{p,P}$ = 4.8 kJ K^{-1} mol^{-1}. (B) Calculated temperature-induced changes of the fractional population of unbound and native PDZ2, unbound and unfolded PDZ2, unbound peptide RG, and the PDZ2/GR complex.

absorption peak whose temperature of maximum heat absorption (which can be regarded as the apparent transition temperature or melting temperature, $T_{m,C}$) is higher by ~6 °C than the melting temperature of PDZ2 alone. Hence, PDZ2 is stabilized in the complex. The dissociation of the complex and the concurrent unfolding of the protein are taking place within a relatively narrow temperature interval.

What can be learned from the thermogram? Figure 6 shows the expected heat capacity of the system in a hypothetical state without intermolecular interactions. This function, C_p^{SUM}, was calculated by simple algebraic summation of the heat capacities of free PDZ2 and free RG; i.e., $C_p^{SUM} = C_p^{PDZ2} + C_p^{RG}$. Between 5 and 30 °C C_p^{SUM} is higher than the heat capacity of the (partly) associated state, $C_p^{PDZ2/RG}$. This reflects the negative heat capacity change accompanying binding. The difference $C_p^{PDZ2/RG} - C_p^{SUM}$ is ~−1.6 ± 0.15 kJ K^{-1} mol^{-1} on average and is thus very close to $\Delta C_{p,A}$ obtained by ITC. However, the close correspondence of the two numbers is perhaps a fortituous coincidence in view of the uncertainties in determination of the absolute heat capacities at relatively low concentrations and the use of calculated partial specific volumes. Much more important for the following discussion is the fact that the slopes of $C_p^{PDZ2/RG}$ and C_p^{SUM} are very close to each other: 96 ± 5 and 112 ± 7 J K^{-2} mol^{-1}, respectively (Table 3). These values imply, in principle, a temperature-dependent $\Delta C_{p,A}$. However, the integral $\int_T (C_p^{PDZ2/RG} - C_p^{SUM})\, dT$ is a small number, and the resulting deviation of the dH_A/dT plot from linearity is certainly lower than the accuracy of the measurements. It follows that the formation of the PDZ2/RG complex is not linked to detectable temperature-dependent structural changes, or at least such changes contribute to the enthalpy of association but do not induce significant temperature dependence of ΔC_p.

The apparent calorimetric enthalpy of complex melting and dissociation, $\Delta H_{cal,PDZ2/RG}$, can be obtained by integration of the heat absorption peak above the chemical baseline constructed in the usual way and amounts to 370 ± 30 kJ mol^{-1} (mean ± SD of three experiments). Integration in respect to ln$T$ yields the apparent entropy of the process, $\Delta S_{cal,PDZ2/RG}$ = 1.07 ± 0.09 kJ K^{-1} mol^{-1}. The apparent calorimetric heat capacity change of complex melting and dissociation, $\Delta C_{p,PDZ/RG}$ corresponds to the difference between the pretransitional and posttransitional portions of the trace linearly extrapolated at the apparent melting temperature; it amounts to 6.0 ± 0.8 kJ K^{-1} mol^{-1}. The difficulty in giving a straightforward interpretation of these parameter numbers as representing the sum of protein unfolding and complex dissociation arises from the fact that the distribution of molecular species in the transition zone is not known a priori. To this end, the excess heat capacity function was analyzed by a model which takes into account the temperature-induced changes in the concentration of free and bound native protein, unfolded protein, and free and bound peptide. This analysis combines the energetics of folding of PDZ2 with the energetics of complex formation described above. The deconvolution technique was developed more than 10 years ago (*33*) and was applied to different types of protein−ligand interactions (*32*, *58*−*62*). Figure 6 presents the results of simulations according to the combined eqs 3−14 as outlined in Experimental Procedures. The experimental excess heat capacity profile of the PDZ2/RG mixture is reproduced with parameters that are in good agreement with parameters describing melting of PDZ2 and PDZ2/RG complex formation at 25 °C. Figure 6B shows the calculated population of each molecular species. At the selected concentrations (~250 μM), the system is partly dissociated at low temperatures, and the concentration of the complex gradually decreases upon heating. PDZ2 melting and complex dissociation are tightly coupled. In the transition region, melting of the complex releases small amounts of free folded protein. This is in accord with a reaction order between 1

Table 3: Thermodynamic Parameters Describing Thermal Melting of PDZ2, RG, and the PDZ2/RG Complex Measured by DSC[a]

	T_m (°C)[b]	ΔH_{cal} (kJ mol^{-1})	ΔS_{cal} (J K^{-1} mol^{-1})	ΔC_p (kJ K^{-1} mol^{-1})	dC_p/dT (J K^{-2} mol^{-1})
PDZ2	49.4	273 ± 10	846 ± 30	4.45 ± 0.20	107 ± 5
	55.2	300 ± 12[c]	925 ± 35[c]		
RG		0	0	0	5 ± 5
PDZ2/RG	55.2	370 ± 30	1070 ± 90	6.00 ± 0.60	96 ± 5
PDZ2 + RG					112 ± 7
complex − components	55.2	70 ± 32	145 ± 95	1.55 ± 0.65	−16 ± 8
complex dissociation	55.2	80 ± 40	165 ± 100	1.76 ± 0.70	−18 ± 9

[a] All experiments were performed in 50 mM sodium phosphate and 150 mM NaCl, pH 6.8. [b] Corresponds to the maximum of the C_p/T curve. [c] Parameters calculated by extrapolation.

and 2. Indeed, the reaction order best describing the melting trace is 1.85 (not shown).

With help of the known molar fractions as a function of the temperature (Figure 6B), we can now deconvolute the total enthalpy change ($\Delta H_{cal,PDZ2/RG}$), entropy change ($\Delta S_{cal,PDZ2/RG}$), and heat capacity change ($\Delta C_{p,PDZ2/RG}$) measured upon melting of the PDZ2/RG mixture. The contribution of the peptide to any parameter can be neglected since temperature-induced conformational changes are calorimetrically silent (see the essentially temperature-independent heat capacity function in Figure 6A). The following equations hold at $T_{m,C}$:

$$\Delta H_{cal,PDZ2/RG} = \Delta H_{cal,P}^{T_{mC}} - f_C \Delta H_{cal,A}^{T_{mC}}$$

$$\Delta S_{cal,PDZ2/RG} = \Delta S_{cal,P}^{T_{mC}} - f_C \Delta S_{cal,A}^{T_{mC}}$$

$$\Delta C_{p,PDZ2/RG} = \Delta C_{p,P} - f_C \Delta C_{p,A}^{T_{mC}}$$

The first terms on the right-hand side are the parameters describing PDZ2 unfolding at $T_{m,C}$ and are calculated as $\Delta H_{cal,P}^{T_{mC}} = \Delta H_{cal,P} + \Delta C_{p,P}(T_{m,C} - T_{m,P})$ and $\Delta S_{cal,P}^{T_{mC}} = \Delta S_{cal,P} + \Delta C_{p,P} \ln(T_{m,C}/T_{m,P})$; $\Delta C_{p,P}$ is a constant over the small temperature range of extrapolation. The second terms on the right-hand side are the energetic parameters of the PDZ/RG complex. The minus sign accounts for complex dissociation. The multiplier f_C represents the molar fraction of the complex at 30 °C, i.e., at the onset of the heat absorption peak, and equals 0.89. For the only unknowns in the above equations, one obtains $\Delta H_{cal,A}^{T_{mC}} = -80 \pm 40$ kJ mol^{-1}, $\Delta S_{cal,A}^{T_{mC}} = -165 \pm 100$ kJ K^{-1} mol^{-1}, and $\Delta C_{p,A} = -1.8 \pm 0.8$ kJ K^{-1} mol^{-1}. The free energy change is thus −26 kJ mol^{-1}. These are the thermodynamic parameters of association of the PDZ2/RG complex at 55 °C (open symbols in Figure 5). Although the rules of error propagation place a large uncertainty of the calculated numbers, the correspondence between the mean values of the thermodynamic functions obtained by ITC at lower temperatures and by DSC at 55 °C is surprisingly good in view of the crude approximations underlying the calculations. First, any temperature dependence of ΔC_p is neglected. Second, both molecules are considered to be structurally and energetically invariant in the entire temperature range. Third, there is no robust way to justify the validity of the two-state model, and any possible redistribution of binding modes in the transition region is ignored. Fourth, the implicit assumption is that there are no interactions taking place between the peptide and the protein in its denatured state. Nevertheless, the success of the modeling (based on van't Hoff formalism) and the deduced calorimetric enthalpy, entropy, and heat capacity changes indicate that the thermodynamic parameters obtained by ITC and DSC describe the thermodynamics of RG binding to PDZ2 in a consistent way and that the procedure is a valuable alternative to obtain thermodynamic information about protein−ligand binding at temperatures beyond the usually limited temperature range covered by ITC experiments. More importantly, the procedure allows a reliable interpolation of the binding constant to the physiologically relevant temperature of 37 °C.

Energetic Partitioning of the Binding Affinity. The driving force of RG binding to PDZ2 at 25 °C (and in physiologically relevant temperature range) is the favorable enthalpy change. The same is true for PDZ3 of PSD-95, which is also a class I PDZ domain (*54*). In contrast, favorable entropy change dominates the affinity of peptide binding to syntenin PDZ1 and PDZ2 domains (*19*). The latter two domains exhibit degenerate specificity and bind peptide ligands of classes I, II, and III. Neither of them has a histidine (typical for class I) or a hydrophobic residue (typical for class II) or a tyrosine (typical for class III) at the beginning of helix α2. With the limited data available, it is impossible to interpret or generalize the different enthalpy−entropy signature of class I-specific complexes, as compared to PDZ−peptide complexes with degenerate specificity. From a structural perspective, the large spread of binding enthalpies (−2 to −40 kJ mol^{-1} at 25 °C) and the apparent effective enthalpy/entropy compensation are surprising. First, the interactions anchoring the very C-terminal hydrophobic residue are ubiquitous and conservative. Second, it appears that backbone−backbone hydrogen bonding contributes essentially to the binding affinity in a "nonspecific" manner. Although progress has been made toward prediction of binding affinities and actual design of ligands capable of binding PDZ domains (*63*, *64*), the emergent compatibility of the PDZ binding site with ligands that bind, driven by enthalpy or entropy, or both, could turn out to be an obstacle in the rational optimization of lead compounds for high affinity *and* specificity (*65*).

Structural Parametrization of Energetic Changes. However good the precision of measured thermodynamic parameters might be, they reflect the total energetic changes of the considered system. The challenging problem is indeed to relate energy terms to structural features in order to understand the molecular basis of the binding affinity. Starting from the early 1990s, different approaches have been followed (*41*, *66*−*70*). Among different parametrization schemes, we use here the one developed by Murphy and Freire, which has been extensively tested against experimental data on unfolding and binding and enjoys com-

mensurate popularity (*41*, *42*, *69*). For brevity we henceforth refer to the procedure as M&F (standing for Murphy and Freire; the contribution of numerous members of the Murphy and Freire laboratories to the refinement of the calculation is implicitly acknowledged).

Since the M&F calculations rely on solvent accessibility differences, the structures of the binary complex and its components in their free state should be known at high resolution or should be carefully modeled. The NMR structure of the PDZ2/RG complex was solved [1D5G (*10*)]. The NMR structure of PDZ2 in the unbound form is also available [3PDZ (*11*)]. The five C-terminal residues of RG are ordered in the binding site, yet free RG obtains a random coil conformation according to CD measurements, and therefore, the RG structure extracted from the complex is inadequate to model the free RG conformation. To overcome the problem and, more importantly, to create a consistent set of structures, we performed MD simulations of free PDZ2, free RG, and the PDZ2/RG complex in explicit water. According to the usual criteria (C_α RMSD, radius of gyration, solute−solute and solute−solvent energy terms, intermolecular distances) the MD trajectories were well equilibrated to serve as a model of the dynamic behavior of the complex and its components (not shown). The average NMR and MD structures of the PDZ2/RG complex and its components are very close to each other, the C_α RMSD (secondary structure elements) being between 0.87 and 1.36 Å in cross-comparisons. However, we noted a slight structure contraction of the complex during MD. The change in ASA is relatively small but significant in comparison with the spread of ASA within the NMR ensemble. Therefore, we tested the calculations against both ensembles according to the following reaction schemes:

$$\begin{matrix}\text{free PDZ}\\ \text{PDZ}_{\text{3PDZ}}\text{: model NMR}_{\text{conf}}\\ \text{PDZ}_{\text{free,MD}}\text{: model MD}_{\text{conf}}\end{matrix} + \begin{matrix}\text{free RG}\\ \text{RG}_{\text{free,MD}}\text{: models NMR}\\ \text{RG}_{\text{free,MD}}\text{: models MD}\end{matrix} \xrightarrow[\text{models conf}]{1} \begin{matrix}\text{PDZ/RG}\\ \text{PDZ/RG}_{\text{1D5G}}\text{: models NMR}\\ \text{PDZ/RG}_{\text{MD}}\text{: models MD}\end{matrix}$$

$$\begin{matrix}\text{“binding-competent” PDZ}\\ \text{PDZ}_{\text{1D5G}}\text{: model NMR}_{\text{rb}}\\ \text{PDZ}_{\text{bound,MD}}\text{: model MD}_{\text{rb}}\end{matrix} + \begin{matrix}\text{free RG}\\ \text{RG}_{\text{free,MD}}\text{: models NMR}\\ \text{RG}_{\text{free,MD}}\text{: models MD}\end{matrix} \xrightarrow[\text{models rb}]{2} \begin{matrix}\text{PDZ/RG}\\ \text{PDZ/RG}_{\text{1D5G}}\text{: models NMR}\\ \text{PDZ/RG}_{\text{MD}}\text{: models MD}\end{matrix}$$

Reaction 1 represents the real process, taking into account the conformational changes of the protein domain accompanying binding, while reaction 2 is a hypothetical process, where binding is approximated as a rigid-body association. In model NMR, ensemble 3PDZ (human PDZ2) was used to represent the free protein, while the binding-competent conformation was extracted from the structure of the human PDZ2/RG complex (1D5G), which serves also as a model of the associated state of the system. In model MD, the structures of the free and binding-competent PDZ2 were taken from the trajectories of the free protein and of the complex, respectively. In both models, the free peptide was modeled with the MD structure. The calculated surfaces represent averages over the corresponding ensembles.

The calculated parameters are listed in Table 4. The comparison with the experimental parameters is done at 25 and 60 °C for ΔH_A and at 18 °C for ΔS_A, where the total entropy contribution is zero. Model NMR_{conf} predicts the binding enthalpy within the range of the other model's estimates, yet all other terms are significantly different and completely contradict the experimental trend. As noted by Walma et al., the free PDZ2 structure suffers significant problems according to several established structure quality tests (*71*). However, no improvement was achieved by using the NMR structure of the mouse, highly homologous PDZ2 domain (1GM1). The failure of the NMR_{conf} model reiterates that the quality of structures is critical in ASA-based parametrization and warns against the use of homologous structures. Since model NMR_{rb} predicts endothermic binding at 25 °C, we focus the following discussion on the results obtained with the MD ensembles.

Table 4: Calculated and Experimental Energetics of RG Binding to PDZ[a]

	NMR_{rb}[b]	NMR_{conf}[c]	MD_{rb}[d]	MD_{conf}[e]	exp
ΔC_p (kJ K^{-1} mol^{-1})	−0.56	0.16	−0.65	−0.76	−1.44
ΔH at 25 °C (kJ mol^{-1})	8	−7	−9	−15	−40
ΔH at 60 °C (kJ mol^{-1})	−11	−2	−31	−41	−88
ΔS at 18 °C (J K^{-1} mol^{-1})	15	nd	45	80	0
total dehydration part	185	−45	245	300	
total conformational part	−135	nd	−165	−185	
rotation/translation	−35	nd	−35	−35	

[a] In all calculations the MD ensemble of RG was used as the model of the unbound state of the peptide. [b] With the NMR ensemble extracted from the human PDZ/GR complex (1D5G) as the model of the unbound protein. [c] With the NMR ensemble of the free human PDZ2 (3PDZ) as the model of the unbound protein. [d] With the MD ensemble of PDZ2 extracted from the simulation of the PDZ2/GR complex. [e] With the MD ensemble of PDZ2 simulated in the unbound state.

Model MD_{conf} is closest to the experiment in terms of ΔH and ΔC_p, indicating that the transition from the free to the binding-competent state is likely to make an energetic contribution to binding. Comparison of the numbers listed in Table 4 leads to the conclusion that the M&F model underestimates $\Delta C_{p,A}$ and ΔH_A at all temperatures and predicts a positive ΔS_A at 18 °C. The magnitude of the absolute deviations from the experiment, ∼0.5−0.7 kJ K^{-1} mol^{-1} ($\Delta C_{p,A}$), 30−35 kJ mol^{-1} (ΔH_A at 25 °C), and 40−80 J K^{-1} mol^{-1} (ΔS_A at 18 °C), could be considered as representing the inherent inaccuracy of structure-based predictions of the enthalpy and heat capacity changes in protein unfolding (both large in comparison to binding parameters), when applied to a large set of data (experimental values taken from ref *50*). On the other hand, however, the enthalpy of binding of small ligands and protein−protein interactions could be predicted with very high precision (*69*, *72*, *73*). Noteworthy, the parametrization scheme developed by Makhatadze and Privalov (*49*) using different ideas and methodology yields essentially the same overall picture: it predicts $\Delta C_{p,A}$ within 0.6−0.9 kJ K^{-1} mol^{-1} and ΔH_A within −10 to −20 kJ mol^{-1} at 25 °C and significantly overestimates the temperature where ΔS_A crosses zero. Hence, it appears that the experimental parameters "in excess" over the structural prediction are caused by some physical process intimately coupled to binding. Where could the observed

discrepancies stem from? A couple of possibilities are discussed below.

(A) Heat Capacity Change. Experimental ΔC_p values more negative than those predicted from surface burial have been reported for a variety of systems. Apart from the "trivial" case, where large refolding transitions accompanying binding contribute to the apparent ΔC_p change, different explanations have been forwarded with a common theme: The changes in hydration are not the only physical source of ΔC_p decrease concomitant with binding. Additional contributions have been ascribed to (i) small structural perturbations leading to redistribution of easily excitable vibrational modes (*74*), (ii) ligand-induced narrowing of the distribution of enthalpic microstates (*75*), (iii) formation of highly cooperative arrays of noncovalent bonds (*76*), (iv) unusually large temperature dependence of the intrinsic heat capacities of the associated and dissociated states of the system (*77*), and (v) entrapment of water at the binding interface (*78*, *79*). Propositions i−iii represent general concepts that are difficult to verify experimentally. We find no experimental support for proposition iv because the heat capacity of the complex and the sum of the heat capacities of RG and PDZ2 change almost in parallel with temperature (Table 3 and Figure 6). Significant contribution from water entrapment is also unlikely since the contribution of a trapped water molecule to ΔC_p was estimated as being lower than -40 J K^{-1} mol^{-1} in an nonpolar environment (*79*, *80*) and could probably not exceed -75 J K^{-1} mol^{-1} (the heat capacity of bulk water). One to three waters have been detected so far in PDZ−peptide complexes by crystallography, and the residence time of each individual water molecule observed in our MD simulations was never longer than 3.5 ns.[2]

(B) Enthalpy Change. We observe no measurable net heats from protonation/deprotonation events. Also, no ions are present at the protein−peptide interface on the time scale of the MD simulations. The enthalpic effect of the water molecules found at or close to the interface (one on average over the 15 ns MD trajectory) cannot be sizable (*81*, *82*). Hence, the structure-based prediction underestimates the generic binding enthalpy (*41*, *42*). It should be noted that eq 16 relates the enthalpy (of unfolding) to the average packing density of proteins and assumes no residual enthalpy after breakage of all relevant noncovalent bonds. We have estimated the packing density by calculating the energy-weighted distance average between atom−atom pairs which form the typical array of noncovalent bonds in proteins and protein−protein complexes (*81*). The obtained values are much larger than those for the reference set analyzed in ref *81* and, hence, indicate substantially looser packing of the PDZ2/RG interface in comparison with the interior of an average protein. Furthermore, the hydrogen bonds at the interface are not particularly short or geometrically optimized, or networked, and visual inspection does not identify other polar interactions that might explain a strong enthalpic effect. We conclude that the experimental ΔH_A contains a contribution of an exothermic process that is not related to the formation of intermolecular contacts.

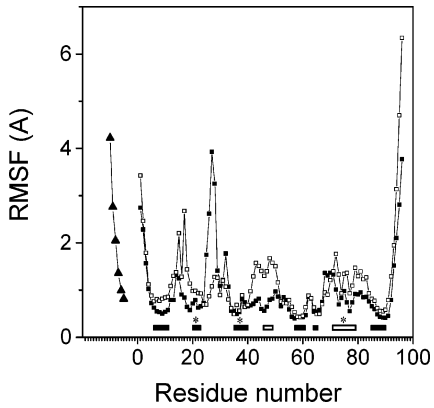

FIGURE 7: Root mean square fluctuations (RMSF) of the C_α atoms around the average MD structures. Shown is RMSF of unbound PDZ2 (open symbols), bound PDZ2 (filled symbols), and bound RG (triangles). Only RMSF of the six C-terminal residues of RG (positions -5 to 0; left to right) are plotted. Secondary structure elements are represented with filled bars (β-strands) and open bars (α-helices). The asterisks indicate secondary structure elements that form the peptide binding site (strands $\beta 2$ and $\beta 3$ and α-helix 2; left to right).

(C) Entropy Changes. At 18° ΔS_A is zero and, therefore, the total dehydration contribution is precisely balanced by the total conformational entropy change plus the loss of rotational/translational degrees of freedom (eq 17). The latter term is still a matter of much debate. Following M&F for consistency, we use here -35 J K^{-1} mol^{-1}, which is close to the cratic entropy and has been found to describe reasonably the loss of rotational/translational degrees of freedom in diverse experimental systems (*44*−*46*). The M&F model predicts "excess" positive entropy (favoring binding). In fact, the calculated conformational entropy (disfavoring binding) is perhaps an overestimate. In the calculation of the conformational contribution we have conservatively assigned the ΔS_{bb} and ΔS_{ex-u} terms to all five peptide residues that appear structured in the binding pocket. The entropy loss arising from backbone immobilization (ΔS_{bb}) tabulated in ref *41* should possibly be reduced for all RG residues, since packing at the binding site is looser than in an average protein, and the thermal motions of the peptide are not significantly restricted (Figure 7). The conclusion is that there must be a source of negative entropy counterbalancing the positive entropy of surface dehydration. Similarly to ΔC_p and ΔH, water entrapment is not the likely contributor.

Tightening of PDZ2 Possibly Contributes to the Energetic Profile of the PDZ2/RG Complex. Altogether, the comparison between experiment and prediction could be interpreted with the presence of a molecular process manifested by an exothermic heat effect, which is linked to an entropy loss and a negative heat capacity change. The energetic expenditure of the overall structural rearrangement of the free components within the complex, where PDZ2 and RG are in the binding-competent conformations, appears to be small (compare the results of the rb and conf models). Qualitatively, the energetic picture might possibly indicate structural tightening of the PDZ2 domain as the consequence of RG binding. Closer packing intensifies enthalpic interactions, but a more rigid and less fluctuating complex is disfavored

[2] Usually, water molecules are involved in the coordination of the C-terminal carboxylate of the incoming peptide within the carboxylate binding loop. In our MD simulations the carboxylate of Val 0 is bonded to the side chain of Asn 16 via a water bridge during 9 ns of the total 15 ns of simulation. For an additional 2 ns a water-mediated bridge is seen with the backbone amide of Gly 19. Water occasionally bridges also the carbonyl group of Ala -1 with the guanidine group of Arg 79.

entropically. The associated heat capacity decrement is not very large since the proposed subtle increase in packing affects mostly buried residues and does not include changes in hydration. A quantitative treatment of the data is not possible to evaluate the associated free energy change, but with the numbers taken at face value from Table 4, it appears that enthalpic stabilization dominates over entropic destabilization at 25 °C. The deduced energetic signature might represent thermodynamic manifestation of the more general concept that "stiffening" of a receptor and cooperativity in ligand binding are two faces of the same phenomenon, as proposed by Cooper and Dryden (*83*) and more recently discussed in detail by Williams et al. in the light of new experimental findings (ref *84* and references cited therein). The experimental evidence for ligand-induced structural tightening of the PDZ2 domain is circumstantial at present. Visual inspection of Figure 7 reveals a uniform sequential distribution of regions with reduced dynamics. Peptide binding to PDZ2 causes depression of the local unfolding/breathing rate around helix α1, far away from the peptide binding site (*17*). Significant change in PDZ2 dynamics upon binding was demonstrated on the basis of spin relaxation measurements (*18*). Coupling between binding and changes in the collective dynamics of the domain was also identified by normal mode analysis (*85*). Long-range residue−residue coupling was detected very recently by pump−probe MD simulations (*86*). Fuentes et al. found that the residues which are dynamically affected are clustered in two regions, both distal from the binding site (*18*). The connectivity pattern of residues undergoing changes in dynamics closely resembles the pattern of statistical couplings that has been identified in the PDZ domain family from multiple sequence analysis (*87*). Statistically significant, correlated, and evolutionarily conserved couplings between residues occupying remote protein regions are thought to reflect a mechanism of allosteric regulation and/or cooperativity without large-scale conformational rearrangement. In physical terms, however, the relevant indicator of long-range interactions is the existence of energetic, i.e., thermodynamic couplings. At least in one case of the PDZ family, many statistically coupled positions are in fact thermodynamically coupled (*87*). On the basis of the qualitative agreement between residue dynamics and thermodynamic residue−residue coupling, Fuentes et al. plausibly suggest modulation and diversification of the functional role of PDZ domains through long-range communication between the peptide binding site and "secondary, distal surfaces". Alternatively, localized (or global) response of the PDZ domain may represent a general mechanism to enhance or weaken binding (*84*). The enthalpy−entropy balance of such long-range energetic coupling is not known. It should be noted that statistical couplings describe a protein fold as a whole and must not hold for individual family members; i.e., statistical couplings (a family property) must not translate equally in thermodynamic coupling (a family member property). Moreover, in view of the generally low sequence homology in the PDZ family, the strength of thermodynamic coupling is likely to vary from one family member to another. It is tempting to speculate that the different energetic signature of PDZ−peptide complexes, as discussed above, originates in part from differences in the energetic balance of subtle structural response of PDZ domains to peptide binding.

ACKNOWLEDGMENT

We thank V. Sathya Devi for the preparation of peptide samples and Serge Chesnov for mass spectrometry measurements and amino acid analysis.

REFERENCES

1. Sheng, M., and Sala, C. (2001) PDZ domains and the organization of supramolecular complexes, *Annu. Rev. Neurosci. 24*, 1−29.
2. Bezprozvanny, I., and Maximov, A. (2001) PDZ domains: More than just a glue, *Proc. Natl. Acad. Sci. U.S.A. 98*, 787−789.
3. Hung, A. Y., and Sheng, M. (2002) PDZ domains: Structural modules for protein complex assembly, *J. Biol. Chem. 277*, 5699−5702.
4. Montell, C. (2000) A PDZ protein ushers in new links, *Nat.e Genet. 26*, 6−7.
5. Nourry, C., Grant, S. G. N., and Borg, J.-P. (2003) PDZ domain proteins: Plug and play!, *Sci. STKE 2003*, re7.
6. Sherman, D. L., Fabrizi, C., Gillespie, C. S., and Brophy, P. J. (2001) Specific disruption of a Schwann cell dystrophin-related protein complex in a demyelinating neuropathy, *Neuron 30*, 677−687.
7. Verpy, E., Leibovici, M., Zwaenepoel, I., Liu, X. Z., Gal, A., Salem, N., Mansour, A., Blanchard, S., Kobayashi, I., Keats, B. J. B., Slim, R., and Petit, C. (2000) A defect in harmonin, a PDZ domain-containing protein expressed in the inner ear sensory hair cells, underlies Usher syndrome type 1C, *Nat. Genet. 26*, 51−55.
8. Bezprozvanny, I., and Maximov, A. (2001) Classification of PDZ domains, *FEBS Lett. 509*, 457−462.
9. Birrane, G., Chung, J., and Ladias, J. A. A. (2003) Novel mode of ligand recognition by the erbin PDZ domain, *J. Biol. Chem. 278*, 1399−1402.
10. Kozlov, G., Banville, D., Gehring, K., and Ekiel, I. (2002) Solution structure of the PDZ2 domain from cytosolic human phosphatase hPTP1E complexed with a peptide reveals contribution of the beta 2-beta 3 loop to PDZ domain-ligand interactions, *J. Mol. Biol. 320*, 813−820.
11. Kozlov, G., Gehring, K., and Ekiel, I. (2000) Solution structure of the PDZ2 domain from human phosphatase hPTP1E and its interactions with C-terminal peptides from the Fas receptors, *Biochemistry 39*, 2572−2580.
12. Skelton, N. J., Koehler, M. F. T., Zobel, K., Wong, W. L., Yeh, S., Pisabarro, M. T., Yin, J. P., Lasky, L. A., and Sidhu, S. S. (2003) Origins of PDZ domain ligand specificity: structure determinationand mutagenesis of the Erbin PDZ domain, *J. Biol. Chem. 278*, 7645−7654.
13. Tochio, H., Hung, F., Li, M., Bredt, D. S., and Zhang, M. J. (2000) Solution structure and backbone dynamics of the second PDZ domain of postsynaptic density-95, *J. Mol. Biol. 297*, 830−830.
14. Erdmann, K. S., Kuhlmann, J., Lessmann, V., Herrmann, L., Eulenburg, V., Muller, O., and Heumann, R. (2000) The adenomatous polyposis coli-protein (APC) interacts with the protein tyrosine phosphatase PTP-BL via an alternatively spliced PDZ domain, *Oncogene 19*, 3894−3901.
15. Kim, E., DeMarco, S. J., Marfatia, S. M., Chishti, A. H., Sheng, M., and Strehler, E. E. (1998) Plasma membrane Ca^{2+} ATPase isoform 4b binds to membrane-associated guanylate kinase (MAGUK) proteins via their PDZ (PSD-95/Dlg/ZO-1) domains, *J. Biol. Chem. 273*, 1591−1595.
16. Songyang, Z., Fanning, A. S., Fu, C., Xu, J., Marfatia, S. M., Chishti, A. H., Crompton, A., Chan, A. C., Anderson, J. M., and Cantley, L. C. (1997) Recognition of unique carboxyl-terminal motifs by distinct PDZ domains, *Science 275*, 73−77.
17. Ekiel, I., Banville, D., Shen, S. H., and Gehring, K. (1998) Effect of peptide binding on amide proton exchange rates in the PDZ2 domain from human phosphatase hPTP1E, *Biochem. Cell. Biol. 76*, 334−340.
18. Fuentes, E. J., Der, C. J., and Lee, A. L. (2004) Ligand-dependent dynamics and intramolecular signaling in a PDZ domain, *J. Mol. Biol. 335*, 1105−1115.
19. Kang, B. S., Cooper, D. R., Jelen, F., Devedjiev, Y., Derewenda, U., Dauter, Z., Otlewski, J., and Derewenda, Z. S. (2003) PDZ tandem of human syntenin: Crystal structure and functional properties, *Structure 11*, 459−468.
20. Niethammer, M., Valtschanoff, J. G., Kapoor, T. M., Allison, D. W., Weinberg, R. J., Craig, A. M., and Sheng, M. (1998) CRIPT,

a novel postsynaptic protein that binds to the third PDZ domain of PSD-95/SAP90, *Neuron 20*, 693−707.
21. Lu, J., Li, H., Wang, Y., Sudhof, T. C., and Rizo, J. (2005) Solution structure of the RIM1[alpha] PDZ domain in complex with an ELKS1b C-terminal peptide, *J. Mol. Biol. 352*, 455−466.
22. Freiss, G., and Vignon, F. (2004) Protein tyrosine phosphatases and breast cancer, *CRC Oncol. Hematol. 52*, 9−17.
23. Palmer, A., Zimmer, M., Erdmann, K. S., Eulenburg, V., Porthin, A., Heumann, R., Deutsch, U., and Klein, R. (2002) EphrinB phosphorylation and reverse signaling: Regulation by Src kinases and PTP-BL phosphatase, *Mol. Cell 9*, 725−737.
24. Sato, T., Irie, S., Kitada, S., and Reed, J. C. (1995) FAP-1: a protein tyrosine phosphatase that associates with Fas, *Science 268*, 411−415.
25. Murthy, K. K., Clark, K., Fortin, Y., Shen, S.-H., and Banville, D. (1999) ZRP-1, a zyxin-related protein, interacts with the second PDZ domain of the cytosolic protein tyrosine phosphatase hPTP1E, *J. Biol. Chem. 274*, 20679−20687.
26. Gao, X., Satoh, T., Liao, Y., Song, C., Hu, C.-D., Kariya, K.-i., and Kataoka, T. (2001) Identification and characterization of RA-GEF-2, a Rap guanine nucleotide exchange factor that serves as a downstream target of M-Ras, *J. Biol. Chem. 276*, 42219−42225.
27. Plotnikov, V. V., Brandts, J. M., Lin, L. N., and Brandts, J. F. (1997) A new ultrasensitive scanning calorimeter, *Anal. Biochem. 250*, 237−244.
28. Freire, E. (1995) Thermal denaturation methods in the study of protein folding, *Methods Enzymol. 259*, 144−169.
29. Freire, E., and Biltonen, R. L. (1978) Statistical mechanical deconvolution of thermal transitions in macromolecules. I. Theory and application to homogeneous systems, *Biopolymers 17*, 463−479.
30. Privalov, P. L., and Potekhin, S. A. (1986) Scanning microcalorimetry in studying temperature-induced changes in proteins, *Methods Enzymol. 131*, 4−51.
31. Privalov, P. L., and Makhatadze, G. I. (1990) Heat capacity of proteins. II. Partial molar heat capacity of the unfolded polypeptide chain of proteins: Protein unfolding effects, *J. Mol. Biol. 213*, 385−391.
32. Milev, S., Gorfe, A. A., Karshikoff, A., Clubb, R. T., Bosshard, H. R., and Jelesarov, I. (2003) Energetics of sequence-specific protein-DNA association: Binding of integrase Tn916 to its target DNA, *Biochemistry 42*, 34813491.
33. Brandts, J. F., and Lin, L. N. (1990) Study of strong to ultratight protein interactions using differential scanning calorimetry, *Biochemistry 29*, 6927−6940.
34. Bashford, D. (2004) Macroscopic electrostatic models for protonation states in proteins, *Front. Biosci. 9*, 1082−1099.
35. Lindahl, E., Hess, B., and van der Spoel, D. (2001) GROMACS 3.0: a package for molecular simulation and trajectory analysis, *J. Mol. Model. 7*, 306−317.
36. Jorgensen, W. L., Chandrasekhar, J., Madura, J. D., Impey, R. W., and Klein, M. L. (1983) Comparison of simple potential functions for simulating liquid water, *J. Chem. Phys. 79*, 926−935.
37. Hess, B., Bekker, H., Berendsen, H. J. C., and Fraaije, J. G. E. M. (1997) LINCS: A linear constraint solver for molecular simulations. *J. Comp. Chem. 18*, 1463−1472.
38. Miyamoto, S., and Kollman, P. A. (1992) Settle - an analytical version of the shake and rattle algorithm for rigid water models, *J. Comput. Chem. 13*, 952−962.
39. Darden, T., York, D., and Pedersen, L. (1993) Particle mesh Ewald−an N.Log(N) method for Ewald sums in large systems, *J. Chem. Phys. 98*, 10089−10092.
40. Berendsen, H. J. C., Postma, J. P. M., Vangunsteren, W. F., Dinola, A., and Haak, J. R. (1984) Molecular-dynamics with coupling to an external bath, *J. Chem. Phys. 81*, 3684−3690.
41. Baker, B. M., and Murphy, K. P. (1998) Prediction of binding energetics from structure using empirical parameterization, *Methods Enzymol. 295*, 294−315.
42. Luque, I., and Freire, E. (1998) Structure-based prediction of binding affinities and molecular design of peptide ligands, *Methods Enzymol. 295*, 100−127.
43. Hubbard, S. J., and Thornton, J. M. (1993) NACCESS, Computer Program, Department of Biochemistry and Molecular Biology, University College, London.
44. Yu, Y. B., Privalov, P. L., and Hodges, R. S. (2001) Contribution of translational and rotational motions to molecular association in aqueous solution, *Biophys. J. 81*, 1632−1642.
45. Antonsson, P., Kammerer, R. A., Schulthess, T., Hanisch, G., and Engel, J. (1995) Stabilization of the alpha-helical coiled-coil domain in laminin by C-terminal disulfide bonds, *J. Mol. Biol. 250*, 74−79.
46. Bardi, J. S., Luque, I., and Freire, E. (1997) Structure-based thermodynamic analysis of HIV-1 protease inhibitors, *Biochemistry 36*, 6588−6596.
47. Gomez, J., Hilser, V. J., Xie, D., and Freire, E. (1995) The heat capacity of proteins, *Proteins: Struct., Funct., Genet. 22*, 404−412.
48. Gianni, S., Calosci, N., Aelen, J. M. A., Vuister, G. W., Brunori, M., and Travaglini-Allocatelli, C. (2005) Kinetic folding mechanism of PDZ2 from PTP-BL, *Protein Eng., Des. Sci. 18*, 389−395.
49. Makhatadze, G. I., and Privalov, P. L. (1995) Energetics of protein structure, *Adv. Protein Chem. 47*, 307−425.
50. Robertson, A. D., and Murphy, K. P. (1997) Protein structure and the energetics of protein stability, *Chem. Rev. 97*, 1251−1267.
51. Haynie, D. T., and Freire, E. (1994) Estimation of the folding/unfolding energetics of marginally stable proteins using differential scanning calorimetry, *Anal. Biochem. 216*, 33−41.
52. Myers, J. K., Pace, C. N., and Scholtz, J. M. (1995) Denaturant m-values and heat-capacity changes−relation to changes in accessible surface-areas of protein unfolding, *Protein Sci. 4*, 2138−2148.
53. Gianni, S., Engstrom, A., Larsson, M., Calosci, N., Malatesta, F., Eklund, L., Ngang, C. C., Travaglini-Allocatelli, C., and Jemth, P. (2005) The kinetics of PDZ domain-ligand interactions and implications for the binding mechanism, *J. Biol. Chem. 280*, 34805−34812.
54. Saro, D., Klosi, E., Paredes, A., and Spaller, M. R. (2004) Thermodynamic analysis of a hydrophobic binding site: Probing the PDZ domain with nonproteinogenic peptide ligands, *Org. Lett. 6*, 3429−3432.
55. Marfatia, S. M., MoraisCabral, J. H., Kim, A. C., Byron, O., and Chishti, A. H. (1997) The PDZ domain of human erythrocyte p55 mediates its binding to the cytoplasmic carboxyl terminus of glycophorin C−Analysis of the binding interface by in vitro mutagenesis, *J. Biol. Chem. 272*, 24191−24197.
56. Gopalakrishnan, M., Forsten-Williams, K., Cassino, T., Padro, L., Ryan, T., and Tãuber, U. (2005) Ligand rebinding: self-consistent mean-field theory and numerical simulations applied to surface plasmon resonance studies, *Eur. Biophys. J. 34*, 943−958.
57. Nieba, L., Krebber, A., and Pluckthun, A. (1996) Competition BIAcore for measuring true affinities: Large differences from values determined from binding kinetics, *Anal. Biochem. 234*, 155−165.
58. Carra, J. H., and Privalov, P. L. (1997) Energetics of folding and DNA binding of the MAT alpha homeodomain, *Biochemistry 36*, 526−535.
59. Celej, M. S., Dassie, S. A., Gonzalez, M., Bianconi, M. L., and Fidelio, G. D. (2006) Differential scanning calorimetry as a tool to estimate binding parameters in multiligand binding proteins, *Anal. Biochem. 350*, 277−284.
60. Mitkevich, V. A., Schulga, A. A., Ermolyuk, Y. S., Lobachov, V. M., Chekhov, V. O., Yakovlev, G. I., Hartley, R. W., Nick, Pace, C., Kirpichnikov, M. P., and Makarov, A. A. (2003) Thermodynamics of denaturation of complexes of barnase and binase with barstar, *Biophys. Chem. 105*, 383−390.
61. Plotnikov, V., Rochalski, A., Brandts, M., Brandts, J. F., Williston, S., Frasca, V., and Lin, L. N. (2002) An autosampling differential scanning salorimeter instrument for studying molecular interactions, *Assay Drug Dev. Technol. 1* (Part 1), 83−90.
62. Waldron, T. T., and Murphy, K. P. (2003) Stabilization of proteins by ligand binding: Application to drug screening and determination of unfolding energetics, *Biochemistry 42*, 5058−5064.
63. Rupasinghe, C. N., and Spaller, M. R. (2006) The interplay between structure-based design and combinatorial chemistry, *Curr. Opin. Struct. Biol. 10*, 1−6.
64. Wiedemann, U., Boisguerin, P., Leben, R., Leitner, D., Krause, G., Moelling, K., Volkmer-Engert, R., and Oschkinat, H. (2004) Quantification of PDZ domain specificity, prediction of ligand affinity and rational design of super-binding peptides, *J. Mol. Biol. 343*, 703−718.
65. Ruben, A. J., Kiso, Y., and Freire, E. (2006) Overcoming roadblocks in lead optimization: A thermodynamic perspective, *Chem. Biol. Drug Des. 67*, 2−4.

66. Cummings, M. D., Hart, T. N., and Read, R. J. (1995) Atomic solvation parameters in the analysis of protein-protein docking results, *Protein Sci. 4*, 2087−2099.
67. Horton, N., and Lewis, M. (1992) Calculation of the free-energy of association for protein complexes, *Protein Sci. 1*, 169−181.
68. Krystek, S., Stouch, T., and Novotny, J. (1993) Affinity and specificity of serine endopeptidase protein inhibitor interactions−Empirical free-energy calculations based on X-ray crystallographic structures, *J. Mol. Biol. 234*, 661−679.
69. Luque, I., and Freire, E. (2002) Structural parameterization of the binding enthalpy of small ligands, *Proteins: Struct., Funct., Genet. 49*, 181−190.
70. Williams, D. H., Cox, J. P. L., Doig, A. J., Gardner, M., Gerhard, U., Kaye, P. T., Lal, A. R., Nicholls, I. A., Salter, C. J., and Mitchell, R. C. (1991) Toward the semiquantitative estimation of binding constants−Guides for peptide peptide binding in aqueous solution, *J. Am. Chem. Soc. 113*, 7020−7030.
71. Walma, T., Spronk, C. A. E. M., Tessari, M., Aelen, J., Schepens, J., Hendriks, W., and Vuister, G. W. (2002) Structure, dynamics and binding characteristics of the second PDZ domain of PTP-BL, *J. Mol. Biol. 316*, 1101−1110.
72. Baker, B. M., and Murphy, K. P. (1997) Dissecting the energetics of a protein-protein interaction: the binding of ovomucoid third domain to elastase, *J. Mol. Biol. 268*, 557−569.
73. Lavigne, P., Bagu, J. R., Boyko, R., Willard, L., Holmes, C. F., and Sykes, B. D. (2000) Structure-based thermodynamic analysis of the dissociation of protein phosphatase-1 catalytic subunit and microcystin-LR docked complexes, *Protein Sci. 9*, 252−264.
74. Sturtevant, J. M. (1977) Heat-capacity and entropy changes in processes involving proteins, *Proc. Natl. Acad. Sci. U.S.A. 74*, 2236−2240.
75. Eftink, M., and Biltonen, R. L. (1980) Thermodynamics of interaction biological systems., in *Biological Microcalorimetry* (Beezer, A. E., Ed.) pp 343−412, Academic Press, San Diego, CA.
76. Cooper, A., Johnson, C. M., Lakey, J. H., and Nollmann, M. (2001) Heat does not come in different colours: entropy-enthalpy compensation, free energy windows, quantum confinement, pressure perturbation calorimetry, solvation and the multiple causes of heat capacity effects in biomolecular interactions, *Biophys. Chem. 93*, 215−230.
77. Privalov, G. P., and Privalov, P. L. (2000) Problems and prospects in microcalorimetry of biological macromolecules, *Methods Enzymol. 323*, 31−62.
78. Cooper, A. (2005) Heat capacity effects in protein folding and ligand binding: A re-evaluation of the role of water in biomolecular thermodynamics, *Biophys. Chem. 115*, 89−97.
79. Morton, C. J., and Ladbury, J. E. (1996) Water mediated protein-DNA interactions: The relationship of thermodynamics to structural detail, *Protein Sci. 5*, 2115−2118.
80. Connelly, P. R. (1997) *The Cost of Releasing Site-Specific, Bound Water Molecules from Protein: Towards a Quantitative Guide for Structure-Based Drug Design*, Springer, Berlin.
81. Hilser, V. J., Gomez, J., and Freire, E. (1996) Enthalpy change in protein folding and binding: Refinement of parameters for structure-based calculations, *Proteins: Struct., Funct., Genet. 26*, 123−133.
82. Holdgate, G. A., Tunnicliffe, A., Ward, W. H. J., Weston, S. A., Rosenbrock, G., Barth, P. T., Taylor, I. W. F., Pauptit, R. A., and Timms, D. (1997) The entropic penalty of ordered water accounts for weaker binding of the antibiotic novobiocin to a resistant mutant of DNA gyrase: A thermodynamic and crystallographic study, *Biochemistry 36*, 9663−9673.
83. Cooper, A., and Dryden, D. T. F. (1984) Allostery without conformational change. A plausible model, *Eur. Biophys. J. 11*, 103−109.
84. Williams, D. H., Stephens, E., O'Brien, D. P., and Zhou, M. (2004) Understanding noncovalent interactions: Ligand binding energy and catalytic efficiency from ligand-induced reductions in motion within receptors and enzymes, *Angew. Chem., Int. Ed. 43*, 6596−6616.
85. De Los Rios, P., Cecconi, F., Pretre, A., Dietler, G., Michielin, O., Piazza, F., and Juanico, B. (2005) Functional dynamics of PDZ binding domains: A normal-mode analysis, *Biophys. J. 89*, 14−21.
86. Sharp, K., and Skinner, J. J. (2006) Pump-probe molecular dynamics as a tool for studying protein motion and long range coupling, *Proteins: Struct., Funct., Bioinf. 65*, 347−361.
87. Lockless, S. W., and Ranganathan, R. (1999) Evolutionarily conserved pathways of energetic connectivity in protein families, *Science 286*, 295−299.

BI061869I